AIAA 80-0181R

Steady and Unsteady Vortex-Induced Asymmetric Loads on Slender Vehicles

L. E. Ericsson and J. P. Reding
Lockheed Missiles and Space Company, Inc., Sunnyvale, Calif.

Nomenclature

b = wing span
c = reference length, $c=d$ for bodies
$C_{m\alpha}$ = $\partial C_m/\partial\alpha$; $C_{\ell\beta}=\partial C_\ell/\partial\beta$
D = drag, coefficent $C_D=D/(\rho_\infty U_\infty^2/2)S$
d' = sectional drag, coefficient $c_d=d'/(\rho_\infty U_\infty^2/2)c$
d = maximum diameter for body of revolution
$\bar{d}$ = mean diameter, $\bar{d}=\int_0^l 2\,r\,d(x/\ell)$
J = blowing momentum, coefficient $c_\mu=J/(\rho_\infty U_\infty^2/2)S$
l = body length
l_0 = forebody length forward of rotation center (Fig. 8)
l_N = nose length
ℓ = rolling moment, coefficient $C_\ell=\ell/(\rho_\infty U_\infty^2/2)S\bar{b}$
L = vortex wake wave length
M = Mach number
M_p = pitching moment, coefficient $C_m=M_p/(\rho_\infty U_\infty^2/2)Sc$
n = yawing moment, coefficient $C_n=n/(\rho_\infty U_\infty^2/2)Sc$
N = normal force, coefficient $C_N=N/(\rho_\infty U_\infty^2/2)S$
p_N = nose tip roll rate
q = pitch rate
Re = Reynolds number based on $d_{\max}$ and freestream conditions; usually $Re=R_d$
R_d = Reynolds number, $R_d=U_\infty d/\nu_\infty$
S = reference area, $S=\pi d^2/4$
$\bar{S}$ = reference area (= projected wing area)
t = time
U = velocity
x = axial body-fixed coordinate (distance from apex)
Y = side force, coefficient $C_Y=Y/(\rho_\infty U_\infty^2/2)S$
α = angle of attack
$\dot{\alpha}$ = $\partial\alpha/\partial t$; $C_{\dot{\phi}'}=\partial C_m/\partial\dot{\phi}'\,l_0/U_\infty)$
β = sideslip angle
γ = rotation of plane of symmetry of forebody vortices (Fig. 8)
θ_c = cone half-angle
θ_A = apex half-angle
ρ = air density
ϕ = roll angle
ϕ' = coning angle (Fig. 8)
ϕ_s = three-dimensional separation angle (Fig. 15)
σ' = total angle of inclination (Fig. 8)
ν = kinematic viscosity
ω = angular rate

Subscripts

A = apex
AM = effective apex angle
AV = asymmetric vortices
c = cone
n = normal to body axis
N = nose
P = port side
s = separated flow
S = starboard
SV = symmetric vortices
UV = unsteady vortices
v = vortex
W = wall
∞ = freestream conditions

Introduction

THE continually increasing performance demands on present day aircraft and missiles have brought on intensive research aimed at providing the needed understanding of the vehicle aerodynamics at high angles of attack where separated flow vortices often have a dominating influence. Recently there has been a series of papers reviewing the state of the art for the prediction of these high-α aerodynamics.[1-5] Nielsen[1,2] concentrated his attention on the existing capability of predicting the missile aerodynamics at high angles of attack where the effects of symmetric vortices

Lars E. Ericsson is a Senior Consultant Engineer in the Engineering Technology organization where he acts as a consultant to Satellite and Missile Systems Divisions on problems associated with aeroelasticity and vehicle dynamics. Before joining Lockheed Aircraft Corporation in 1956, and LMSC in 1959, he was with the Aeronautical Research Institute of Sweden and the Swedish Aircraft Company, SAAB. Dr. Ericsson received his MS Degree from the Royal Institute of Technology (KTH), Stockholm, in 1949, and his Ph.D. in 1972. He is an Associate Fellow of the American Institute of Aeronautics and Astronautics and is a member of the American Helicopter Society. Dr. Ericsson has published more than 100 papers in his related fields.

Pete Reding, an Associate Fellow of AIAA, has had roughly 22 years experience in the aerospace industry working generally in the field of unsteady aerodynamics. He was first mystified by body vortex effects during his two-and-a-half years at what was then Douglas Aircraft Company, where he worked immediately after graduation from the University of Michigan in 1958. Now at Lockheed Missiles and Space Co., Inc. (since 1961) he has wrestled with separated flows, booster aeroelastic stability, airfoil stall, the dynamics of bulbous based bodies, ablating bodies, shuttle vehicles, decelerators, dynamic support interference, and aeroacoustics. Not one to give up easily he has once again attacked the mysteries of body vortices.

Presented as Paper 80-0181 at the AIAA 18th Aerospace Sciences Meeting, Pasadena, Calif., Jan. 14-16, 1980; submitted Jan. 30, 1980; revision received June 30, 1980.

from the forebody and its canard surfaces on aft body and fins have demanded major new analytical/experimental efforts. Wardlaw[3] and Jorgensen[4] expanded the coverage to include the large effects of asymmetric forebody vortices on the lateral missile aerodynamics, which in turn was the prime topic of the most recent review by Chapman and Keener.[5] The present paper extends the scope from the static aerodynamics considered earlier[1-5] to an in-depth study of the unsteady aerodynamics associated with symmetric and asymmetric vortex shedding on aircraft and missiles.

Background

As a slender body is pitched through the angle-of-attack range $0 \leq \alpha \leq 90$ deg, it experiences four distinct flow patterns that reflect the diminishing influence of the axial component. At low angles of attack ($0 \leq \alpha < \alpha_{SV}$), the axial flow dominates and the flow is attached. At intermediate angles of attack ($\alpha_{SV} \leq \alpha < \alpha_{AV}$), crossflow sweeps the boundary layer to the leeward side where it separates and rolls up into a symmetric vortex pair. At high angles of attack ($\alpha_{AV} \leq \alpha < {}_{UV}$), crossflow effects start to dominate and the vortices become asymmetric thereby producing a side force at zero sideslip. Finally, at very high angles of attack ($\alpha_{UV} \leq \alpha \leq 90$ deg), the crossflow dominates completely and the boundary layer is shed in the form of a Kármán vortex street or random wake depending upon Reynolds number, Mach number, geometric details, and so forth. These different flow regions were discovered by Allen and Perkins,[6] and their gradual development has been described in detail by Fiechter[7] using exquisite flow visualization results to illustrate the various flow patterns.

On pointed, slender cones development of symmetric vortices has been observed when the angle of attack exceeds the cone half-angle, both for laminar and turbulent flow, and at all speeds from incompressible flow to hypersonic velocities.[8,9] In laminar flow the value is $\alpha_{SV} \approx 1.1\,\theta_c$, whereas the turbulent value is $\alpha_{SV} \approx 1.3\,\theta_c$. Asymmetric vortex shedding starts when the angle of attack exceeds the total included angle at the apex[10,11] (i.e., $\alpha_{AV} \approx 2\,\theta_A$).

Whereas the angle α_{SV} seems to be rather insensitive to Mach number,[12] the angle α_{AV} varies greatly with Mach number[10,13-15] (Fig. 1). For not so slender noses, $\theta_A > 20$ deg, α_{AV} is determined mainly by the body fineness ratio, l/d. Fiechter[7] observed asymmetric vortex shedding to start at station x when $\alpha = 4.2\ d/x$. Thus, one would expect that $\alpha_{AV} \leq 4.2\ d/l$. This value is approached asymptotically by the experimental results in Refs. 10 and 16 for large l/d. The unsteady vortex shedding starts at $\alpha \leq 60$ deg.

Asymmetric Vortices in Three-Dimensional Flow

In three-dimensional flow the asymmetric von Kármán-type vortex geometry can be realized in a steady-state condition, as has been pointed out by Thomson and Morrison[17] and by Pick.[18] The axial flow degree of freedom makes this possible. The analogy is, however, strictly valid only for blunt-nosed cylinders. For bodies with slender, pointed noses the first asymmetric vortex pair is generated by the nose in a manner quite different from that described in Ref. 17, as will be discussed in more detail later.

Effect of Reynolds Number and Roughness

As expected, Reynolds number has a dominating influence on the side force induced by asymmetric vortices. The results by Keener et al.[16] Nelson and Fleeman,[11] and Smith[19] have been analyzed to obtain the maximum C_Y to C_N ratio as a function of the effective Reynolds number[20] (see Fig. 2). It can be seen that there exists a critical Reynolds number giving the maximum $|C_Y|/C_N$ ratio. It is also evident that this critical Reynolds number varies from one angle of attack to the next and from one test to the next (in different wind tunnels). The maximum side force will be realized at a Reynolds number where boundary-layer transition can influence the flow separation aysmmetry the most (see the discussion of two-dimensional Magnus effects in Ref. 21). It is clear that this Reynolds number will vary greatly from tunnel to tunnel due to the well-known problem of tunnel noise effects on boundary-layer transition.[22,23] That the critical Reynolds number can vary from one α to the next is less obvious. However, the vortex-generating forebody is pitched to a different proximity to the tunnel ceiling with its noisy boundary layer. This may play an important role in generating the observed α-effect on the critical Reynolds number.

Considering the large effect of Reynolds number one expects, of course, that surface roughness will have a large effect; and it does, as experimental results[24] illustrate. It is apparent that the large effect of forebody roll orientation has its roots in some form of nose tip imperfections. This effect of roll angle was observed already by Gowen and Perkins.[25] It has since then been observed by others.[18,26,27] It is discussed in Ref. 28 how one, through small changes of the nose geometry, can reduce greatly and even eliminate the vortex-induced side loads.

Effect of Mach Number

Wardlaw and Morrison have reviewed the effect of Mach number on the vortex-induced maximum side force on cones, tangent-ogives, and parabaloids[29] (Fig. 3). Significant side forces have been measured on sharp cone-cylinders at $M_\infty = 2$ by Atraghji.[27] The effect of crossflow Mach number, $M_n = M_\infty \sin\alpha$, shows a certain similarity to those for two-dimensional flow.[21] That is, at $M_n > 0.5$ the large vortex asymmetry, the supercritical/subcritical flow separation geometry, cannot be established. This fact is also well-illustrated by Magnus force measurements on cylinders in three-dimensional and two-dimensional flow[30] (Fig. 4), and is in basic agreement with the observed disappearance of the

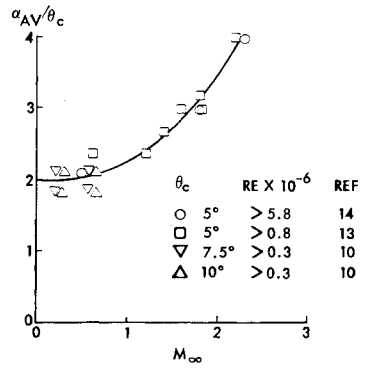

Fig. 1 Angle of attack for starting asymmetric vortex shedding on cones at subsonic and supersonic Mach numbers.

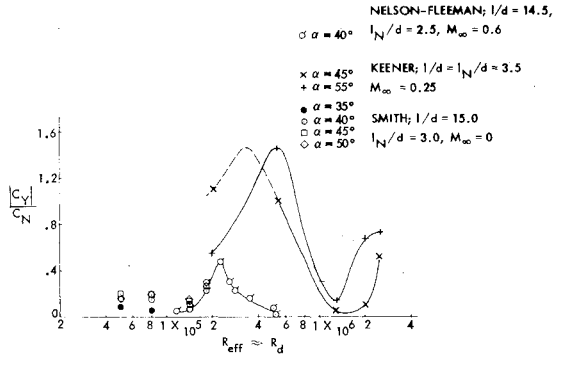

Fig. 2 Critical Reynolds number for maximum vortex-induced side force.

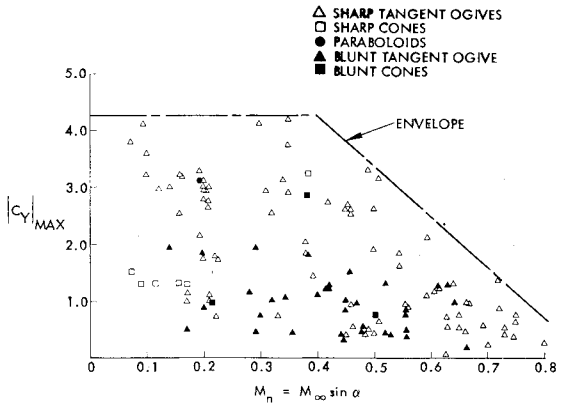

Fig. 3 Effect of crossflow Mach number on maximum vortex-induced side force.[29]

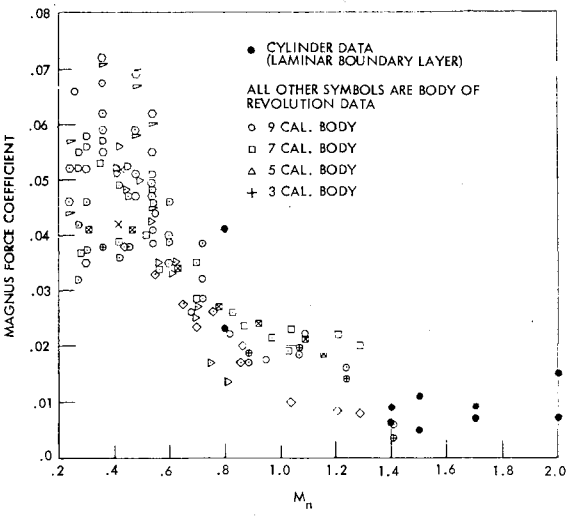

Fig. 4 Comparison of Magnus force data for a cylinder and bodies of revolution.[30]

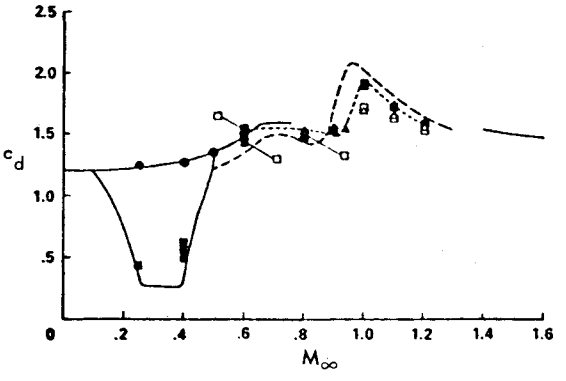

Fig. 5 Effect of Mach number on cylinder drag.[31]

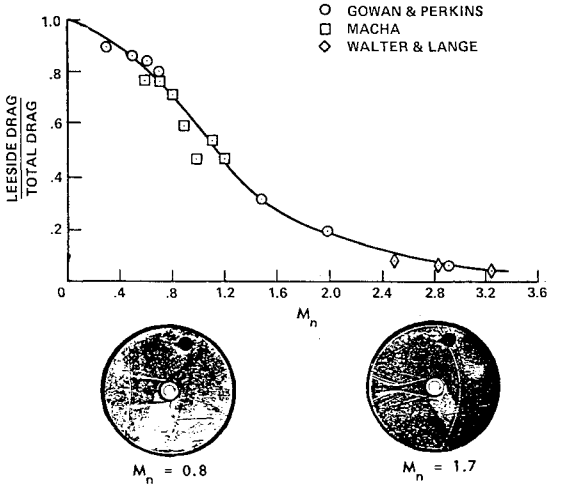

Fig. 6 Subsonic and supersonic base drag and wake flow.

supercritical "drag bucket" at $M>0.5$ (see Ref. 31 and Fig. 5).

There is also a purely three-dimensional reason for the transonic falloff of vortex-induced loads, and that is nose-induced flow separation. It occurs on blunt-nosed bodies already at $\alpha=0$, and will at angle of attack occur even on moderately slender noses.[32-34] This three-dimensional, closed separation bubble prevents the nose from generating the vortices associated with open separation regions, that play such an important part in the vortex induced asymmetric (and symmetric) loads at lower subsonic Mach numbers. Thus, the vortices can only be generated by the aft body, and the generated side force will, as a consequence, be relatively small. The flow pattern observed at $M_\infty=2.45$ on a flat-nosed cylinder at high angles of attack[35] shows nose-induced flow separation followed by aftbody vortices, that first are symmetric and then become asymmetric, all in agreement with the vortex geometry specified by Thomson.[36] Very similar characteristics have been observed on a hemisphere cylinder.[35]

On a very slender nose tip the nose-induced separation phenomenon does not occur, and consequently, nose-generated asymmetric vortices generate significant side forces also at supersonic speed, as is demonstrated by Atraghji's 5.7 deg cone-cylinder data,[27] and is illustrated further by Rainbird's 5 deg cone data.[14] The increasing importance of the nose slenderness with increasing Mach number is well illustrated by the data in Fig. 2 for incipient asymmetric vortex shedding. One notices that no significant vortex-induced side loads have been observed at supersonic crossflow Mach numbers.[14,27,30,36,37] The reason for this is twofold. The leeside contribution to the total drag decreases fast with increasing cross flow Mach number[2] (Fig. 6). In addition, it becomes more and more difficult to generate a force through differential (top and bottom side) base pressure. Platou's flow pictures,[30] inserted in Fig. 6, show that there is simply no effective area over which the asymmetric separation can generate a significant side load at $M_n>1$.

Moving Wall Effects

As in the two-dimensional flow case[21] moving wall effects will be important also for axisymmetric bodies at high angles of attack.

Effect of Spin

At low spin rates the response of the side force to the varying roll position of the body-fixed asymmetry is almost instantaneous, and no consistent effect of the spin rate can be seen. The data in Ref. 38 indicate that this is also the case at somewhat higher spin rates, up to 6⅓ Hz, but still with surface velocities only a few percent of freestream speed. There is a sign of a small time-lag effect in realizing the vortex-induced side load, and a similar phase-lag effect can also be deduced from the data in Ref. 27. Experimental data for a cone[39] (Fig. 7) demonstrate the effect of viscous flow time lag. Using the convective time lag derived in Ref. 40, one predicts a spin-induced distortion of the transition front that is in good agreement with the experimental results in Fig. 7. Combining the methods of Refs. 40 and 41, one finds that both this transition-front distortion and the flow-separation geometry are determined by the flow conditions at apex at an earlier time, $t_0-\Delta t$. At moderate angles of attack this

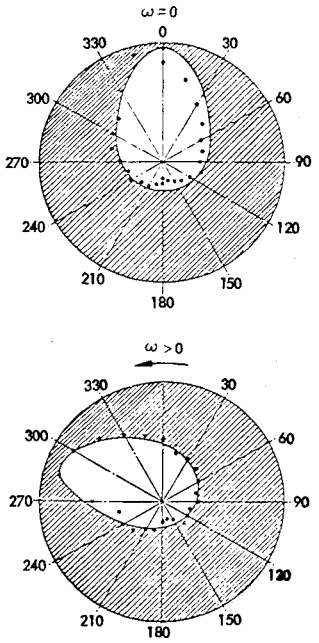

Fig. 7 Effect of spin rate on boundary-layer transition on a 10 deg cone at $\alpha = 4$ deg and $M_\infty = 2$ (Ref. 39).

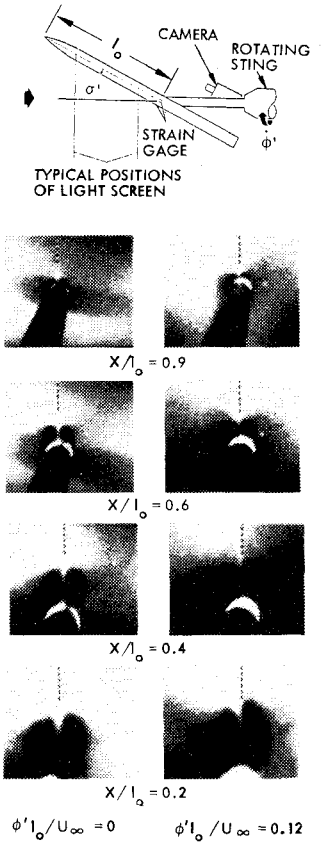

Fig. 8 Effect of coning motion on the vortex geometry of an ogive-cylinder at $M_\infty = 1.4$ (Ref. 42).

phenomenon will play an important role in the generation of asymmetric flow separation and associated vortices on very slender noses.

Effect of Coning Rate

How the coning motion affects free body vortices was first shown by Tobak et al.[42] (Fig. 8). The symmetric nose-generated vortex pair is tilted an angle $\gamma = \tan^{-1}(\dot{\phi}' l_0/U_\infty)$,

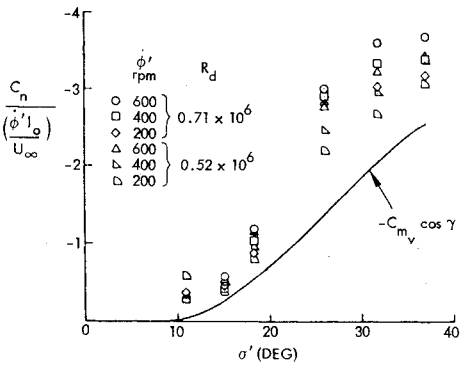

Fig. 9 Side moment coefficient due to coning motion of an ogive-cylinder at $M_\infty = 1.4$ (Ref. 42).

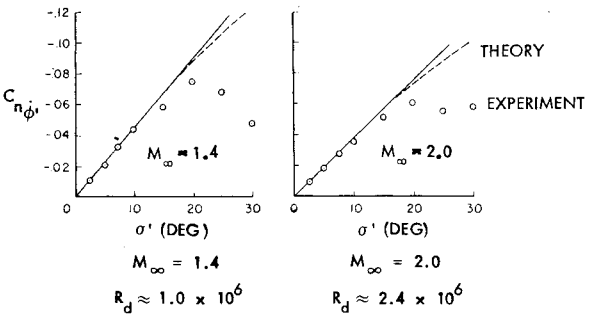

Fig. 10 Yawing moment coefficient for a coning 10 deg sharp cone at $M_\infty = 1.4$ and 2.0 (Ref. 43).

the crosswind-induced tilt angle at apex. The angle at which the vortices are tilted remains the same regardless of x-station,* i.e., the apex conditions are controlling the downstream vortex location. By tilting the vortex-induced pitching moment vector (obtained from static tests) through the angle γ, the predicted side moment characteristics shown in Fig. 9 were obtained. It can be seen that the main portion of the experimentally determined side moment due to coning rate is predicted in this manner. The remaining difference is probably induced by vortex asymmetry. Figure 8 shows the vortex lobe to be larger on the advancing than on the retreating side. This can be explained by the moving wall effects discussed in Ref. 21, that promote separation on the advancing side, resulting in an increased vortex, whereas the effects are the opposite for the retreating side. The same type of tests have later been performed for a 10 deg sharp cone[43] (Fig. 10). We see again the experimental data deviating from predictions when the vortices can become asymmetric (i.e., for $\alpha/\theta_c > 2$; see Fig. 1). However, in this case the deviation goes in the opposite direction from what was the case for the ogive cylinder (compare Figs. 9 and 10). Going back to the discussion of Magnus effects in Ref. 21, one finds that this reversal should occur if the flow conditions were in the critical Reynolds number range for the cone test, but not for the test with the ogive cylinder. This would also explain the much larger deviation from prediction for the cone.

The stated Reynolds number ranges for the tests are $Re = 0.2\text{-}0.7 \times 10^6$ for the ogive cylinder and $Re = 1.0\text{-}2.4 \times 10^6$ for the cone. The maximum reversal effect in Ref. 21 was obtained at $Re = 0.35 \times 10^6$. Results published recently by Mack[44] show that the transition Reynolds number could increase as much as a factor of 6 when going from the incompressible flow conditions in Ref. 21 to the present supersonic test conditions for the cone[43] (Fig. 10). That is, the maximum reversal should occur at

*Later tests showed this to be true also for body stations downstream of the rotation center.

$Re = 6 \times 0.358 \times 10^6 = 2.1 \times 10^6$, which falls in the test range used, $Re = 1.2\text{-}2.8 \times 10^6$. Going back to Ref. 21, one finds that purely subcritical conditions existed at $Re = 0.358 \times 10^6$, which with a factor of 6 gives $Re = 0.215 \times 10^6$ for the ogive-cylinder test[42] (Fig. 9), falling in the Reynolds number range used in the test, $Re = 0.2\text{-}0.7 \times 10^6$. The 600 rpm coning rate used was high enough to tilt the vortices an angle of 2 deg and should, therefore, overpower any nose asymmetries on a carefully made model, as was confirmed experimentally. The test was run with positive and negative coning rates. No noticeable differences in the data were observed (when the rotation direction was accounted for). Even at 600 rpm the surface velocity ratio U_W/U_∞ is small, being 0.007 and 0.0055 at apex for $\sigma' = 30$ deg at $M_\infty = 1.4$ and $M_\infty = 2.0$, respectively.

Effect of Pitch Rate

As in the case of spin rate just discussed, the effect of pitch rate should be large in the critical Reynolds number region. The results obtained by Smith and Nunn[19] show that this is indeed the case. Figure 11 demonstrates how the subcritical condition can be reached by pitching the body at the constant reduced angular rate $\dot{\alpha}d/U_\infty = 2.7 \times 10^{-3}$ at a supercritical† Reynolds number, $Re = 8 \times 10^4$. This is the reverse moving wall effect discussed in Ref. 21, that delays transition and causes a switch from supercritical to subcritical flow conditions. The pitch rate had no effect on the lateral characteristics. This is the expected result when the body is perfectly symmetric, or when the body asymmetry is in an ineffective roll position. The results obtained by others[45] indicate that the latter could have been the case. They rolled their model and found that pitch rate decreased the side moment for one roll position, increased it for another.

In order to get an appreciation for the magnitude of the pitch rate effects shown in Fig. 11 one can make the following comparison. The data give a normal force derivative

$$\partial C_N \Big/ \partial\left(\frac{c\dot{\alpha}}{U_\infty}\right) \approx 5/2.7 \times 10^{-3} = 1.85 \times 10^3$$

The slender body value is

$$\partial C_N \Big/ \partial\left(\frac{cq}{U_\infty} + \frac{c\dot{\alpha}}{U_\infty}\right) \approx -\frac{l}{d}$$

Using crossflow drag for high α gives a similar magnitude derivative. That is, even for $l/d = 10$ the undamping pitch-rate effect demonstrated in Fig. 11 is two orders of magnitude larger than the damping effect obtained in attached flow.

Effect of Model Support

It is rather obvious that the support system will interfere with the vorties that are shed from the model at least for the standard sting support arrangement.[45] The results obtained by Uselton[46] illustrate this effect of support interference. A discussion of this high-α support interference problem as it pertains to subscale testing of missiles and high-performance aircraft is contained in Ref. 47.

Nose-Induced Asymmetric Vortices

The importance of nose-induced asymmetric vortices has been brought out largely through the investigative efforts directed by Keener and Chapman.[10,16,24,48,49,50] Not only are the side loads induced on noses alone of great magnitude, capable of exceeding the normal force,[24] but also, on bodies with geometric features typical of many tactical missiles, the nose-induced side load can often be the dominating load[10]

†The quoted 6% oscillatory variation of the freestream speed[19] may have been responsible for this early subcritical/supercritical transition.

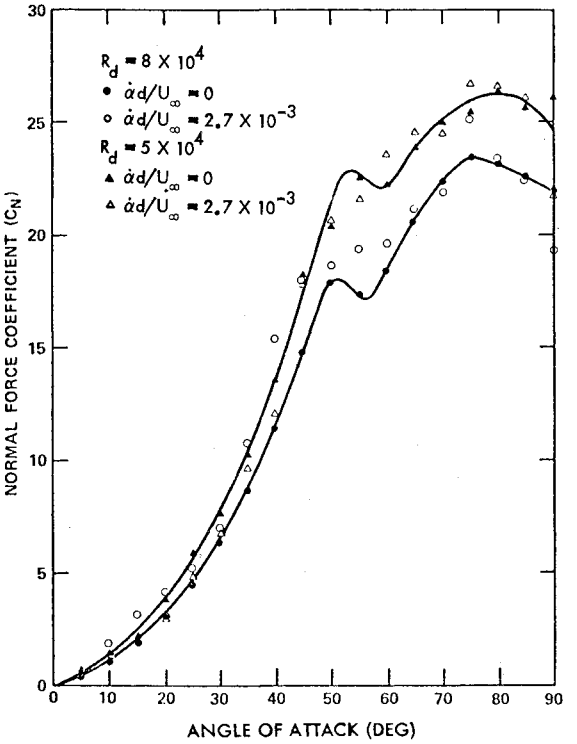

Fig. 11 Effect of pitch rate on the normal force of an ogive-cylinder in the critical Reynolds number region.[19]

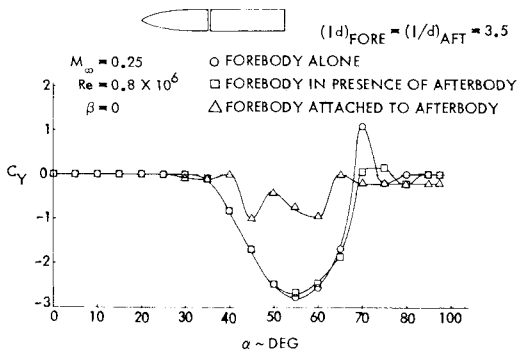

Fig. 12 Effect of cylindrical aftbody on vortex-induced side force of an $l/d = 3.5$ pointed ogive.[10]

(Fig. 12). The results indicate that the asymmetric vortices on the aft body have no influence on the flow over the nose, but that they rather have to "line up" in the pattern set by the dominating aysmmetric vortex pair generated by the nose. The dominant influence of the apex conditions is reflected in the measured side force due to asymmetric vortex shedding[27] (Fig. 13). The fineness ratio is the same for the two nose shapes. However, the apex angle for the tangent ogive nose is $\theta_A = 11.32$ deg and for the conic nose $\theta_A = 5.72$ deg.

This nose-dominated vortex pattern is very different from that suggested for aft body asymmetric vortices.[36] According to the latter, the (local) generation of side force would be associated with a (local) lift loss. On the nose, however, the vortex asymmetry results in an increase of the vortex lift, not a lift loss. This is documented by experimental results for a tangent-ogive body[26] (Fig. 14). The strakes eliminate the vortex asymmetry and, as a result, the normal force is decreased for $\alpha > \alpha_{AV}$ (although the strakes increase the lift for $\alpha < \alpha_{AV}$). The increased lift at vortex asymmetry apparently is realized because the remaining vortex moves inboard, under the lifted-off vortex, as is indicated by flow pictures both for pointed ogives[10,51] and slender delta wings.[52]

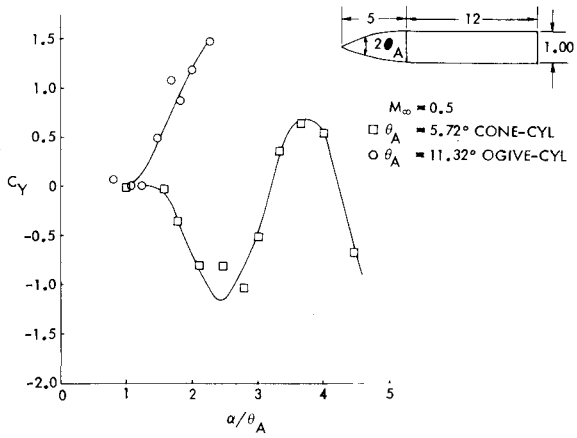

Fig. 13 Effect of apex half-angle on the vortex-induced side force distribution.[27]

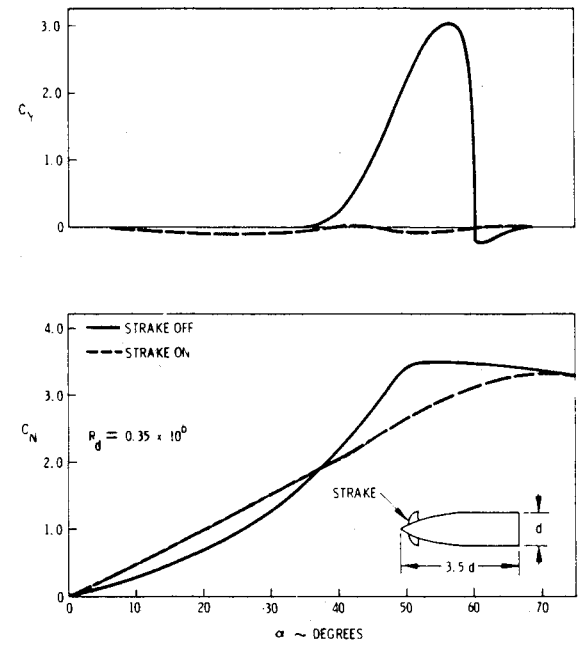

Fig. 14 Comparison of symmetric and asymmetric vortex-induced loads.[26]

It is interesting to compare the separation geometries in Fig. 15 for ogival and conical noses.[53] Because $\alpha/\theta_A = 1.3$, and thus less than α_{AV}/θ_A (Fig. 1), the vortex asymmetry starts developing first on the aft body for the ogive cylinder. For the cone cylinder, on the other hand, $\alpha/\theta_A = 3.1 > \alpha_{AV}/\theta_A$, and the vortex asymmetry starts developing on the nose. When the angle of attack is increased ($\alpha \gg \alpha_{AV}$), appreciable asymmetry starts occurring also on the aft body.[27]

Thus, experimental results indicate that the flow process leading to vortex asymmetry is radically different in the case of a pointed, slender nose from what it is on the cylindrical aft body, the case which until now has received almost all attention, at least in theoretical investigations. It has been noted by Keener and Chapman[54] that the α boundaries for incipient asymmetric loads at zero sideslip are very similar for slender bodies[10] and delta wings[55] when plotted against the fineness ratio. They suggest, therefore, that the vortex asymmetry in both cases is caused by a basic hydrodynamic instability resulting from the "crowding together" of the vortices. They further draw the conclusion that in that case the aysmmetry in the separation points on a body of revolution would not be necessarily an essential feature of vortex asymmetry. The tuft-grid pictures obtained by Bird on narrow delta wings[52] tend to support the conclusion drawn by Keener and Chapman.

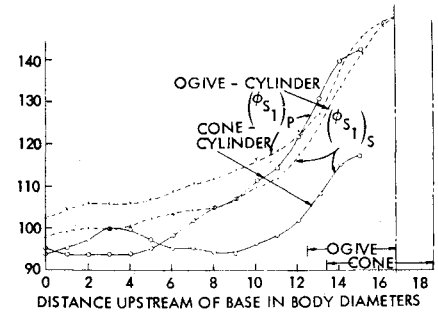

Fig. 15 Comparison of asymmetric primary separation lines on cone-cylinder and ogive-cylinder at $M_\infty = 0.6$ and $R_d = 1.9 \times 10^6$ (Ref. 53).

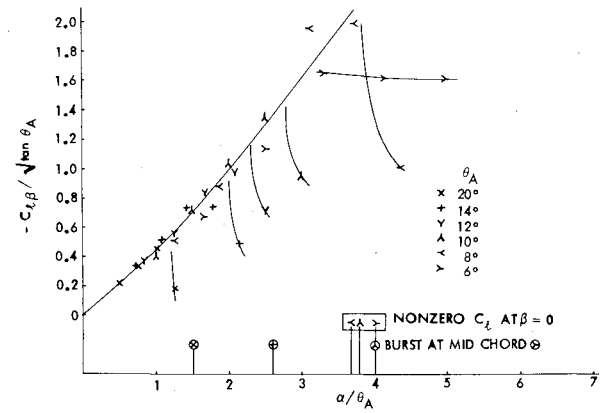

Fig. 16 Correlation of roll stability, vortex asymmetry, and vortex burst for narrow sharp-edged delta wings.

It is clear, then, that asymmetric vortices occur also when the separation point is fixed by the geometry. It is well documented, however, that the generated forces are very much dependent upon the separation point degree of freedom, both in the two-dimensional unsteady case and in the three-dimensional steady case. In two-dimensional flow the translatory oscillations do not affect strongly the vortex shedding unless the separation point is free to move.[21] In the three-dimensional case the separation point degree of freedom is an essential mechanism in the generation of asymmetric loads. One would expect the generated asymmetric forces to be much smaller for the case that the separation point was fixed by the geometry, in complete analogy with the subduing effect that a fixed separation point has on the two-dimensional response.[21]

A well-known vortex instability problem for delta wings is the vortex burst.[56] In Fig. 16 the roll stability derivative ($C_{\ell\beta}$) measured by Shanks[55] is plotted in the normalized form derived in Ref. 57. Also shown is the angle of attack at which significant rolling moment was measured at $\beta = 0$, indicating starting vortex asymmetry,[55] as well as the angle for which vortex burst occurs at midchord.[56] (For narrow-delta wings vortex burst more or less jumps from trailing edge to midchord.) It can be seen that a loss of lateral stability precedes the occurrence of asymmetric vortices, which event in turn precedes the vortex burst. The tiny "fuselage" on the delta wings tested by Shanks[55] is likely to have provided the same effect as the splines investigated by Maltby and Peckham.[58] They found that an addition of a small spline along the leeward meridian promoted early vortex asymmetry both on (flat plate) delta wings and on pointed cones with flat-top cross sections. We have suggested[59] that the reason for this effect is that the flow cannot find a stable stagnation point on top of the centerline spline, forcing the stagnation point to move to one side, thereby causing the vortex asymmetry.

However, even without this center spline, narrow delta wings will develop the vortex asymmetry.[52,56,60] For $\theta_A \geq 15.7$ deg vortex burst will precede vortex asymmetry,[60] and the asymmetric loads will be generated by asymmetric vortex burst at $\alpha/\theta_A > 2.25$ (see Ref. 61).

Analysis

All theoretical efforts to predict the vortex-induced asymmetric loads until now have been based upon inviscid flow modeling of the vortices generated for subcritical conditions on the cylindrical aft body. In full-scale flight the asymmetric loads of concern will occur at critical to supercritical flow conditions and will be produced by asymmetric vortices generated by a pointed, slender forebody. The evidence presented so far shows conclusively that boundary-layer transition plays a dominant role in the generative process of the asymmetric vortices that cause the large side loads of special concern.

The impulsively started cylinder flow analogy, first used by Allen and Perkins,[6] and described more recently by Sarpkaya,[62] who supplies detailed experimental data in support of his analysis, assumes that the crossflow plane is swept down the length of the body at the uniform rate $U_\infty \cos\alpha$. Thus, the developing flow in the crossflow plane is analogous to a two-dimensional cylinder in impulsively started flow with velocity $U_\infty \sin\alpha$. That is, the downstream distance from the start of the inclined cylinder is $x = U_\infty t \cos\alpha$. Sarpkaya's data[62] indicate that for incompressible, subcritical flow ($Re < 1.2 \times 10^6$) the wake asymmetry first develops at $Ut/d = 4$, where $U = U_\infty \sin\alpha$ for the inclined cylinder. Thus, the angle of attack (α_{AV}) for incipient asymmetric vortex shedding, starting at the base ($x = 1$), is

$$\alpha_{AV} = \tan^{-1}[4/(l/d)] \tag{1}$$

Sarpakaya's data also show that the first large vortex is shed at $Ut/d = 8.5$. This gives

$$\alpha_{\text{peak}} = \tan^{-1}[8.5/(l/d)] \tag{2}$$

According to Wardlaw and Morrison,[29] these formulas can be applied to bodies with nonconstant cross section by substituting d by

$$\bar{d} = \int_0^l 2r\,\mathrm{d}\left(\frac{x}{l}\right)$$

For the sharp cone Eqs. (1) and (2) then give

$$\alpha_{AV} = \tan^{-1}(4\tan\theta_c) \approx 4\theta_c$$

and

$$\alpha_{\text{peak}} = \tan^{-1}(8.5\tan\theta_c) \approx 8.5\,\theta_c$$

If $\bar{d} = d$ were used, one would obtain $\alpha_{AV} \approx 2\theta_c$ in agreement with experiment. However, for pointed ogives with $\theta_A = 2\theta_c$ for the same l_N/d one would still obtain $\alpha_{AV} \approx 4\theta_A$, not $\alpha_{AV} \approx 2\theta_A$ the value indicated by experiments.[10,16] Experimental incompressible results define $\alpha_{AV} \approx = 2\theta_c$ (Fig. 1) and show that $\alpha_{\text{peak}} < 2\alpha_{AV}$ for pointed noses, even in presence of a cylindrical aftbody (Fig. 13).

Following a suggestion by Morkovin, Thomson and Morrison[17,36] applied the time-space equivalence between the von Kármán unsteady, asymmetric vortex wake in two-dimensional flow and the steady, asymmetric vortex array in three-dimensional flow. Atraghji[63] modified the Thomson-Morrison method[17,36] by allowing the diameter d and wavelength L to vary with distance x along the body while keeping the ratio d/L constant. This d/L ratio is found by trial and error in matching the experimental data. Figure 17 shows that even then it is not possible to match the experimental data. Whereas the impulsive flow analogy[62] overestimated the experimentally observed angle α_{AV} for incipient asymmetric vortex shedding by a factor of 2, the method based upon the space-time equivalence for the Kármán vortex street[17,36,63] underestimates α_{AV} by a factor of ½ to ⅓. The remaining characteristics for the vortex-induced side loads, α_{peak} and $|C_Y|_{\max}$, cannot be predicted either.

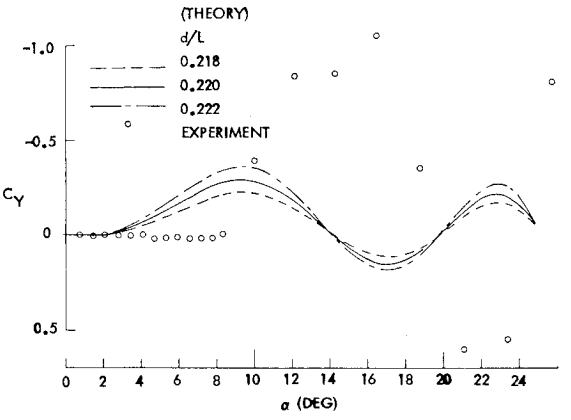

Fig. 17 Comparison between predicted and experimental side force on an $l/d = 17$ cone-cylinder at $M_\infty = 0.5$ and $R_d \approx 1.4 \times 10^6$ (Ref. 63).

The mismatch between theory and experiment, as exemplified by Fig. 17, is not typical when considering more recent modifications.[64-73] However, in addition to introducing the area changing neglected in most theories the slender nose introduces also the dominating-apex feature, which is even harder to simulate theoretically. Only if one recognizes this dominance of the apex is it possible to understand the large alleviating effect of nose bluntness, nose-strakes, nose booms, etc. discussed in Ref. 28. The observed large effect of the roll orientation of the nose tip alone or in combination with various aft bodies further testifies to this nose dominance and illustrates the futility of trying to predict any one member of the family of statistically possible $C_Y(\alpha)$ and $C_n(\alpha)$ characteristics. Our approach therefore has been to develop analytic means for prediction of the envelope that encloses the whole family of such characteristics, i.e., $|C_Y|_{\max} = f(\alpha/\theta_A)$ and associated side moment.[20,74] That the obtained envelope is not unreasonably conservative is demonstrated in Ref. 75 by use of new results[76] and further analysis of old data.[77]

Coupling Between Vortex Shedding and Vehicle Motion

Some examples already have been seen where there is a strong coupling between the vortex shedding and the vehicle motion, e.g., body spin (Fig. 7), body coning motion (Figs. 9 and 10), and body pitching (Fig. 11). In all these cases the coupling effects became especially large when boundary-layer transition was involved. Of course, the static vortex-induced side loads themselves become of extreme magnitude only in the critical flow regime (Fig. 2). The transition process is itself very strongly coupled to the vehicle motion, at all speeds, e.g., in the cases of low speed airfoil dynamics,[78] shock/boundary-layer interaction at transonic speeds,[79,80] or re-entry body dynamics at hypersonic velocities.[40] It is, therefore, no surprise that the effect of spinning or coning motions on the generation of asymmetric vortices and associated side loads become especially large when transition is one of the flow mechanisms involved. This strong coupling between vehicle motion and transition complicates dynamic testing as no boundary-layer tripping device can be used.[80,81]

The "frozen" subcritical-supercritical separation geometry on a cylinder normal to the flow,[76,82] that produced the maximum sectional load[74,75] along the full length of the cylinder, resulted because the short laminar separation bubble

with turbulent reattachment was established only on one side of the cylinder. This is the separation geometry for leading edge stall on airfoils. We have hypothesized that the large dynamic overshoot of the maximum lift for static leading edge stall on a pitching airfoil occurs because the wall-jet effect of the upward moving leading edge wipes out the laminar separation bubble.[83] Recent experiments have confirmed that this is really what happens.[84] The same thing may happen on the cylinder, especially in view of the effects that translatory and longitudinal oscillations have on the two-dimensional flow separation.[21] The Reynolds number hysteresis observed by Kamiya et al.[76] lends further support to the existence of such motion sensitivity. A certain vehicle motion, e.g., a steady-state turn that generates the "right" axial distribution of the local effective flow angle could "lock-in" the maximum static separation asymmetry over an extended part of the vehicle, thereby generating the maximum side load rather than the otherwise expected total load.[74] In addition, one must consider the possibility of oscillatory vortex-induced asymmetric loads. Dynamic asymmetric vortex effects could play an important role in wing rock of advanced performance aircraft[48] and possibly be significant also for advanced missile maneuvers.

One very important effect of the asymmetric vortices is the coupling mechanism they provide between longitudinal and lateral degrees of freedom. Forebody pitching generates side loads on downstream missile body and tail surfaces. As these cross-coupling effects are large, highly nonlinear, often discontinuous, and associated with hysteresis effects, and have especially powerful effects on the vehicle dynamics, they have recently become of great concern to missile and aircraft industry.[85] A summary of our present capability (or lack thereof) in handling these new problems is given in Ref. 48.

Work in Progress or Completed Very Recently

Of the works recently completed the experimental investigation by Kruse et al.[86] provides important new information. A systematic investigation of the effect of rolling various components of an ogive-cylinder body reveals the following. Rotating nose tip alone had as large an effect as rotating the complete nose, or the complete body. Rotating only the cylindrical aft body had very little effect, while a significant change did occur when the body aft of the nose tip was rotated. When the nose was made of one piece, thereby supposedly eliminating some of the microasymmetries at the nose tip junction, rotating the aft body had as large an effect as rotating the nose, tending to indicate that the dominant microasymmetry in this case was the nose-aft body juncture. Very similar results have been obtained for a very blunt ogive-cylinder body,[45] where the nose-body junction provided the important asymmetry. All these results indicate that even if there is a basic asymmetry established at the nose tip, be it of hydrodynamic instability character or of viscous origin, downstream viscous flow effects play an important role in the generation of asymmetric loads. That is, of course, in basic agreement with the observed large effect of Reynolds number.

Lamont's latest results[87] (Fig. 18) for a pointed ogive cylinder, ($l_N/d=2, l/d=6$) add to the already existing data base showing a C_Y dip at the start of the supercritical Reynolds number region (see Fig. 2). In Fig. 19 Lamont's data are compared in more detail with earlier results[50] for a more slender pointed ogive cylinder ($l_N/d=3.5$, $l/d=8.5$). It can be seen that Lamont's C_Y results[87] for $\alpha=55$ deg show the same Reynolds number trend as the data by Keener et al.[50] do for $\alpha=30$ deg. It was earlier discussed that it is the relative attitude α/θ_A that determines when the asymmetric vortex shedding begins. For a pointed ogive θ_A is

$$\theta_A=\tan^{-1}\left[\frac{l_N/d}{(l_N/d)^2-0.25}\right] \tag{3}$$

Thus, with $\alpha_{AV}/\theta_A=2$, the asymmetric vortex shedding starts at $\alpha_{AV}=28$ deg for Lamont's $l_N/d=2$ nose and at $\alpha_{AV}=16$ deg for the $l_N/d=3.5$ nose used by Keener et al. Although the C_Y generation starts on the nose, the aft body carries a significant portion of the load, as is demonstrated by the results in Ref. 86. The center of pressure of C_Y is located at the nose-body shoulder. Representing the ogive-cylinder body by a pointed ogive, i.e., substituting l_N by l in Eq. (3) to determine the effective apex angle, provides the lower bound for θ_A, whereas Eq. (3) provides the upper limit for the effective θ_A value for the ogive-cylinder. The average of these upper and lower bounds gives the following effective or mean value

$$\theta_{AM}=\tfrac{1}{2}\left\{\tan^{-1}\left[\frac{l_N/d}{(l_N/d)^2-0.25}\right]+\tan^{-1}\left[\frac{l/d}{(l/d)^2-0.25}\right]\right\} \tag{4}$$

For Lamont's body $\theta_{AM}=18.7$ deg, and $\alpha=55$ deg gives $\alpha/\theta_{AM}=2.94$. The body used by Keener et al. has $\theta_{AM}=11.4$ deg, which for $\alpha/\theta_{AM}=2.94$ would require $\alpha=33$ deg. Thus, it appears reasonable that Lamont's data for $\alpha=55$ deg show such similarity to Keener's data for $\alpha=30$ deg (Fig. 19). The

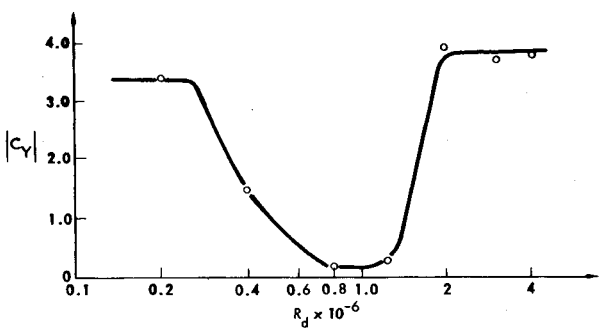

Fig. 18 Variation with Reynolds number of maximum vortex-induced side force of an $l/d=6$ ogive-cylinder at $\alpha=55$ deg.[87]

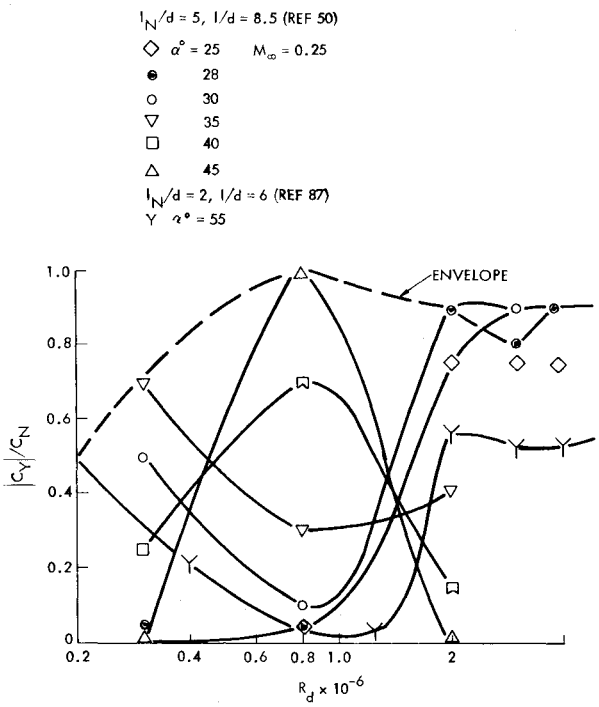

Fig. 19 Effect of *Re* and α on C_Y/C_N of pointed ogive-cylinders.

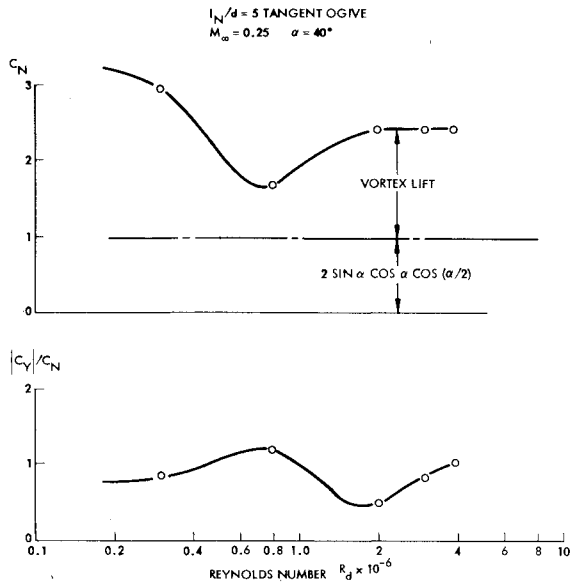

Fig. 20 Variation with Reynolds number of vortex-induced side and normal forces.

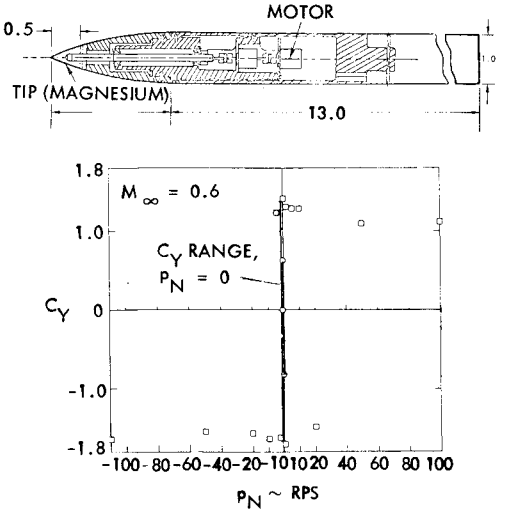

Fig. 21 Effect of a spinning nose tip on the vortex-induced side force of an ogive-cyliner at $\alpha = 55$ deg and $M_\infty = 0.6$ (Ref. 88).

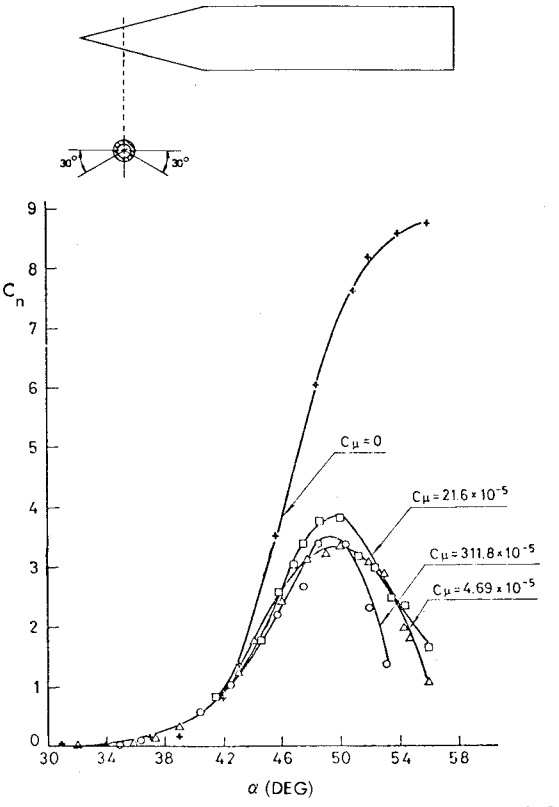

Fig. 22 Effect of windward side nose blowing on the vortex-induced yawing moment of a cone-cylinder body.[93]

dashed line in Fig. 19 shows how the side force ratio $|C_Y|_{max}/C_N$ varies with Reynolds number. $|C_Y|_{max}/C_N$ for the nose itself[50] shows the same Reynolds number trends as the ogive-cylinder body in Fig. 19. Possible reasons for this data trend are discussed in Ref. 75.

Following up on the suggestion made by Chapman and Keener[5] we examine this Reynolds number effect by studying the $C_Y(\alpha)$ and $C_N(\alpha)$ behaviors. It is very apparent that associated with the starting C_Y generation is an increase in C_N (see Ref. 50). The liftoff of one vortex should cause a contribution to C_Y but a loss in C_N. Apparently this liftoff allows the remaining vortex to grow stronger, inducing increased suction that contributes both to C_Y and C_N, with its contribution to C_N overshadowing the C_N loss due to the liftoff of the other vortex. The results for $\alpha = 40$ deg in Ref. 50 are cross plotted as a function of Reynolds number in Fig. 20. If the separated flow geometry remained unchanged with Reynolds number, $|C_Y|/C_N$ would remain constant. It is apparent that the flow separation boundaries change with Reynolds number. It is helpful to compare the results in Fig. 20 with the moving wall effects discussed in Ref. 21. This is done in Ref. 75, and it is shown that the data trends in Fig. 20 can be explained in detail by the observed effects of body rotation and Reynolds number on the flow separation boundaries on a cylinder in two-dimensional flow.

A more direct application of the moving wall effects is found when studying Fidler's very interesting results for ogive-cylinders with spinning nose tips[88] (Fig. 21). At $\alpha = 55$ deg the critical condition discussed for the group 2 data in Ref. 21 was apparently realized in Fidler's test. Thus, the direction of the moving wall dictates the direction of the asymmetric flow separation, causing a jumpwise change of C_Y, similar to the jumpwise change of lift measured by Swanson,[89] that is discussed in Ref. 21. As in the case of the effect of pitch rate measured by Smith[19] (Fig. 11), very modest moving wall velocity can cause a large discontinuous change of the aerodynamic loads. Although the results for a smooth nose tip shown in Fig. 21 are of great basic interest, the main purpose of Fidler's test was to demonstrate that spinning a nosetip that was not smooth, but had large controlled roughness in form of longitudinal grit strips, could alleviate the vortex-induced side loads greatly. The spinning roughness strips could embed the nosetip microasymmetries in a manner somewhat similar to that envisioned for the nose boom effect.[28] Large distributed roughness on the nose tip should have a similar effect, and besides being an alternate fix, brings up the question of how well flight hardware nose tips are represented in subscale tests with a very smooth nose.

Using blowing as a boundary-layer tripping device has been tried successfully by Wallis and others.[90,91] Minute blowing rates, applied in the form of tangential jets in the leading edge region between the stagnation and flow separation points, eliminated the laminar separation bubble and transformed the airfoil stall from the leading edge type to pure turbulent stall. As it has been shown by Chapman and Keener[5,92] that the laminar short bubble definitely is present in the asymmetric vortex shedding process at critical and supercritical Reynolds numbers, the blowing method used by Wallis[90,91] could be applied also to bodies of revolution at high angles of attack. That it indeed can has recently been shown[93] (Fig. 22).

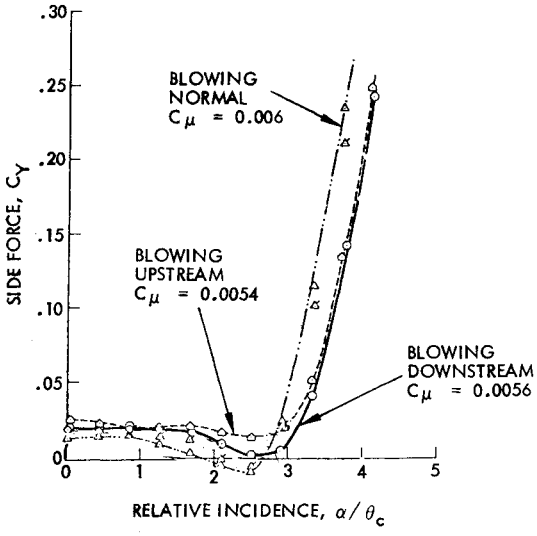

Fig. 23 Effect of various types of leeward side nose blowing on a 5 deg cone at $M_\infty = 0.6$ and $R_d = 2.36 \times 10^6$ (Ref. 98).

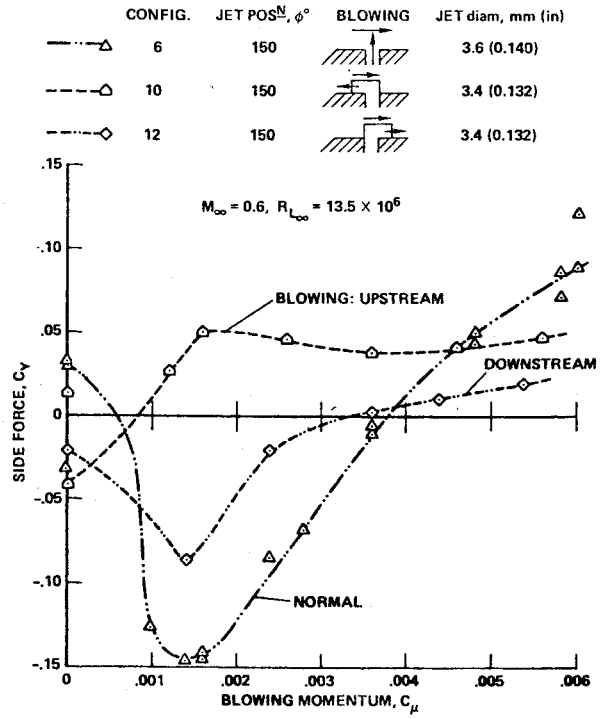

Fig. 24 Effect of blowing momentum on the effectiveness of starboard blowing at $\alpha/\theta_c = 3.2$ (Ref. 98).

Blowing on the windward side 30 deg below the meridian between flow stagnation and separation points did substantially reduce the vortex-induced side moment on an $l/d = 6$ cone-cylinder body. And as in Wallis' case only minute blowing rates are required, $C_\mu < 0.00005$. This symmetric windward side blowing, through the elimination of the laminar separation bubble, makes the separation more securely supercritical, thereby limiting the asymmetry potential (see Ref. 21 and the discussion of group 3 data). Conversely, blowing symmetrically on the top side should cause the separation to change toward the subcritical type (group 1 data in Ref. 21) and should, therefore, increase the asymmetry potential. This is also what the data in Ref. 93 show. Blowing symmetrically on the top side (at 30 or 60 deg above the lateral meridian) did cause an increase in the vortex-induced asymmetric loads. These blowing results[93] reinforce our argument that the flow separation on a slender body at high angles of attack can be coupled to the body motion in the same way as the leading-edge stall is.[94-97]

Asymmetric blowing has been investigated as a means of spin recovery for advanced performance aircraft.[98-100] Peake and Owen[98,99] have made a detailed investigation of the effect of asymmetric blowing near the nose, $x/l = 0.12$, of a 5 deg cone. Already the blowing orifice by itself, without blowing, had a large effect on the side force. As natural transition was occurring at $x/l = 0.20$, the orifice at $x/l = 0.12$ could act as a roughness element, spreading a turbulent wedge downstream[101] that could cause supercritical separation. Changing from normal to tangential blowing, upstream or downstream, had little effect (Fig. 23), again indicating that blowing acts as a "controllable roughness element," as was also suggested by the authors,[98] although they thought such an explanation was overly simplistic.

When looking at the effectiveness of the various normal blowing configurations, the insensitivity to blowing rate for all but one lends strong support to the roughness hypothesis. Looking a little closer at the deviating port-side blowing configuration shows that it too fits the roughness theory (Fig. 24). The result show that all the blowing modes finally give the expected roughness-induced result, at $C_\mu > 0.004$. As expected, upstream blowing is the most effective mode for turbulence generation, reaching full effectiveness at $C_\mu = 0.0015$, and downstream blowing is the least effective. The normal and downstream blowing modes show very irregular data trends for $C_\mu < 0.004$. One would be inclined to ascribe those anomalies to the basic difficulty encountered when trying to determine the incremental effects of blowing using nonrepeatable no-blowing data as a base. As the blowing rate increases its asymmetry potential will finally overpower that of the basic body. Seen in this light the results in Fig. 24 support the roughness hypotheses.

The asymmetric blowing used by Skow et al.[100] is similar to the cone blowing just discussed, but differs in some important aspects. The angles of attack of interest are much larger, $30 < \alpha < 60$ deg rather than $\alpha < 20$ deg, with correspondingly less influence of the axial flow component, and the blowing jet momentum is one to two orders of magnitude larger. The high momentum blowing was applied in the tangential downstream direction under the lifted-off vortex. When the momentum coefficient C_μ was high enough the lifted-off vortex reattached and the opposite vortex lifted off. The mechanism through which the vortex reattachment was accomplished was thought to be mainly entrainment. Apparently, this massive blowing is feasible as a means for (once per flight) spin recovery. The problem with aircraft application of blowing or other devices for control of the vortex asymmetry is that they cannot be applied near the apex because of radar requirements. Application of asymmetric windward mode blowing should provide a much more efficient means of asymmetric vortex control, at least in the spin departure process before the full vortex asymmetry has developed. It is possible that the massive blowing will be needed for spin recovery. Nevertheless, further research should lead to more efficient means for departure prevention and spin recovery.

Conclusions

An assessment of the importance of vortex-induced asymmetric loads on the vehicle dynamics has led to the following conclusions:

A blunt-nosed cylinder at high angle of attack generates a stationary asymmetric vortex array that is similar to the unsteady von Kármán vortex street in two-dimensional flow.

On a pointed, slender body the first asymmetric vortex pair originates at the apex and the former analogy no longer applies. The fluid mechanic instability mechanism leading to the vortex asymmetry instead is likely to be similar to the one existing on narrow delta wings. As in the case of the delta wings the apex angle is the correct normalizing unit for the

effect of angle of attack on the vortex generation. This is true also when the pointed, slender nose is followed by a cylindrical aft body.

The maximum vortex-induced side force occurs at a critical Reynolds number where fully subcritical conditions are reached on one side and fully supercritical on the other.

Surface roughness has a large influence on the vortex-induced asymmetric loads. Invisible, microscopic irregularities in the nose tip region appear to control the asymmetric vortex shedding process, according to the observed effects of rolling the nose tip.

Mach number is a significant parameter. The vortex-induced side loads decrease with increasing subsonic crossflow Mach number above 0.4, and become insignificant at supersonic crossflow Mach numbers.

On a pointed, slender body the vortex-induced asymmetric loads can be reduced greatly and sometimes eliminated completely by use of small nose bluntness, nose boom, nose strakes, or body trips.

Body spin has a significant effect on boundary-layer transition, that in turn plays a dominant role in the generation of large asymmetric loads.

A coning body motion has the effect of tilting the symmetric vortex pair an angle equal to the relative side wind angle at the apex (induced by the coning motion). At an angle of attack near the one where vortex asymmetry occurs in the static case the vortices go asymmetric in a direction determined by the coning motion and the Reynolds number.

Body pitching, like coning, has a large effect on the vortex shedding and associated in-plane loads. In the critical Reynolds number region the pitch rate effects are reversed. The resulting negative damping contribution can be up to two orders of magnitude larger than the attached flow (body alone) positive damping.

Model support interference is often a problem in wind tunnel tests. It is especially difficult in tests of bodies at high angles of attack, where the vortices, which often generate the dominant loads on the model, interact with the downstream support. This problem, that earlier had been ignored both by missile and aircraft industry, is presently getting attention.

Existing theories can usually not predict the experimentally observed aerodynamic characteristics generated by asymmetric vortices. The impulsively started cylinder analogy predicts asymmetric vortex shedding to start at $\alpha_{AV} \approx 4\ \theta_A$, whereas experimental data show $\alpha_{AV} \approx 2\theta_A$. Furthermore, the analogy predicts the vortex generating the largest asymmetric load to be shed at $\alpha_{peak} \approx 8.5\theta_A$, whereas experiments show $\alpha_{peak} < 4\ \theta_A$. In the case of the von Kármán vortex street analogy similar difficulties exist, as there is no means available to represent the pointed nose. Consequently, the nose is more or less ignored in the theoretical developments, whereas experimental evidence shows that it not only generates the largest side load but also greatly influences the asymmetric vortex geometry on the aftbody.

A new method has been developed which uses two-dimensional, unsteady, experimental results to determine the upper bounds for the vortex-induced side loads on an inclined, slender missile body. The boundary determined in this manner bounds all available, experimental, sectional load data.

The coupling between vehicle motion and vortex generation is very significant. When boundary-layer transition occurs, causing the vortex-induced asymmetric loads to reach their peak, the coupling becomes especially strong. It is possible that a particular vehicle maneuver could "lock-in" the maximum crossflow asymmetry over an extended portion of the vehicle thereby potentially increasing the stationary asymmetric loads by 100%. In addition, oscillatory variation of the vortex-induced side loads could play an important role in wing rock of high performance aircraft and could also influence high performance missile dynamics.

One important effect of the asymmetric vortices is to provide a coupling mechanism between longitudinal and lateral degrees of freedom, even at zero sideslip. Forebody pitching generates side forces on downstream missile body and tail surfaces. These cross-coupling effects have been found to be very nonlinear, often discontinuous, and associated with hysteresis effects, with large impact on the vehicle dynamics. They are, for these reasons, presently causing missile and aircraft designers great concern.

Acknowledgments

The paper is in large part based upon the results obtained in a study for NSWC, Silver Spring, Md., Contract N6092177C-0234, under the direction of L.H. Schindel.

References

[1] Nielsen, J.N., "Missile Aerodynamics-Past, Present, Future," *Journal of Spacecraft and Rockets,* Vol. 17, May-June 1980, pp. 165-176.

[2] Nielsen, J.N., "Nonlinearities in Missile Aerodynamics," AIAA Paper 78-20, Jan. 1978.

[3] Wardlaw, A.B. Jr., "High Angle of Attack Missile Aerodynamics," Paper 5, AGARD LS-98, March 1978.

[4] Jorgensen, L.H., "Prediction of Aerodynamic Characteristics for Slender Bodies Alone and With Lifting Surfaces to High Angles of Attack," Paper 28, AGARD CP-247, Sept. 1978.

[5] Chapman, G.T. and Keener, E.R., "The Aerodynamics of Bodies of Revolution at Angles of Attack to 90°," AIAA Paper 79-0023, Jan. 1979.

[6] Allen, H.J. and Perkins, E.W., "Characteristics of Flow Over Inclined Bodies of Revolution," NACA RM A50L07, 1951.

[7] Fiechter, M., "Über Wirbelsysteme an schlanken Rotationskörpern und ihren Einfluss auf die aerodynamischen Beiwerte," Bericht 10/66, Deutsch-Französisches Forchungsinstitut, Sant Louis, France, Dec. 1966.

[8] Rainbird, W.J., "Turbulent Boundary-Layer Growth and Separation on a Yawed Cone," *AIAA Journal,* Vol. 6, Dec. 1968, pp. 2410-2416.

[9] Stetson, K.J. and Ojadana, E.S., "Hypersonic Laminar Boundary Layer Separation on a Slender Cone at Angle of Attack," *AIAA Journal,* Vol. 10, May 1972, pp. 642-648.

[10] Keener, E.R. and Chapman, G.T., "Onset of Aerodynamic Side Forces at Zero Sideslip on Symmetric Forebodies at High Angles of Attack," AIAA Paper 74-770, Aug. 1974.

[11] Nelson, R.C. and Fleeman, E.L., "High Angle of Attack Aerodynamics on a Slender Body with a Jet Plume," *Journal of Spacecraft and Rockets,* Vol. 12, Jan. 1975, pp. 12-16.

[12] Rainbird, W.J., "The External Flow Field About Yawed Circular Cones," Paper 19, AGARD CP-30, AGARD Meeting on Hypersonic Boundary Layers and Flow Fields, London, England, May 1-3, 1968.

[13] Peake, D.J., Owen, F.K., and Higuchi, H., "Symmetrical and Asymmetrical Separations About a Yawed Cone," Paper No. 16, AGARD CP-247, AGARD Symposium on High Angle of Attack Aerodynamics, Sandefjord, Norway, Oct. 4-6, 1978.

[14] Rainbird, W.J., "Private Communication of Unpublished Data on Vortex-Induced Asymmetric Loads on a 5° Cone at Mach Numbers from 0.51 to 4.27," April 5, 1968.

[15] Nebbeling, C. and Bannink, W.J., "Experimental Investigation of Supersonic Flow Past a Slender Cone at High Incidence," *Journal of Fluid Mechanics,* Vol. 87, Pt. 3, Aug. 1978, pp. 475-496.

[16] Keener, E.R., Chapman, G.T., and Kruse, R.L., "Effects of Mach Number and Afterbody Length on Onset of Asymmetric Forces on Bodies at Zero Sideslip and High Angles of Attack," AIAA Paper 76-66, Jan. 1976.

[17] Thomson, K.D. and Morrison, D.F., "The Spacing, Position and Strength of Vortices in the Wake of Slender Cylindrical Bodies at Large Incidence," *Journal of Fluid Mechanics,* Vol. 50, Pt. 4, 1971, pp. 751-783.

[18] Pick, G.S., "Investigation of Side Forces on Ogive-Cylinder Bodies at High Angles of Attack in the M = 0.5 to 1.1 Range," AIAA Paper 71-570, June 1971.

[19] Smith, L.H., "Aerodynamic Characteristics of an Axisymmetric Body Undergoing a Uniform Pitching Motion," Ph.D. Thesis, Naval Post-graduate School, Monterey, Calif., Dec. 1974.

[20] Reding, J.P. and Ericsson, L.E., "Maximum Vortex-Induced Side Force," *Journal of Spacecraft and Rockets,* Vol. 15, July-Aug. 1978, pp. 201-207.

[21] Ericsson, L.E., "Karman Vortex Shedding and the Effect of Body Motion," *AIAA Journal,* Vol. 18, Aug. 1980, pp. 935-944.

[22] Pate, S.R., "Dominance of Radiated Aerodynamic Noise on Boundary Layer Transition in Supersonic and Hypersonic Wind Tunnels, Theory and Application," AEDC TR-77-107, March 1978.

[23] Spangler, J.G. and Wells, C.S. Jr., "Effects of Free Stream Disturbances on Boundary-Layer Transition," *AIAA Journal,* Vol. 3, March 1968, pp. 543-545.

[24] Keener, E.R., Chapman, G.T., Cohen, L., and Taleghani, J., "Side Forces on a Tangent-Ogive Forebody with a Fineness Ratio of 3.5 at High Angles of Attack and Mach Numbers from 0.1 to 0.7," NASA TM X-3437, Feb. 1977.

[25] Gowen, F.E. and Perkins, E.W., "A Study of the Effect of Body Shape on the Vortex Wakes of Inclined Bodies at a Mach Number of 2," NACA RM A53I17, Dec. 1958.

[26] Coe, P.L. Jr., Chambers, J.R., and Letko, W., "Asymmetric Lateral-Directional Characteristics of Pointed Bodies of Revolution at High Angles of Attack," NASA TN D-7095, Nov. 1972.

[27] Atraghji, E.G., "The Influence of Mach Number, Semi-Nose Angle and Roll Rate on the Development of the Forces and Moments Over a Series of Long Slender Bodies of Revolution at Incidence," NAE Data Rept. 5×5/0020, National Research Council, Ottawa, Canada, 1967.

[28] Ericsson, L.E. and Reding, J.P., "Alleviation of Vortex-Induced Asymmetric Loads," *Journal of Spacecraft and Rockets,* Vol. 17, Nov.-Dec. 1980, pp. 548-533.

[29] Wardlaw, A.B. Jr. and Morrison, A.M., "Induced Side Forces at High Angles of Attack," *Journal of Spacecraft and Rockets,* Vol. 13, Oct. 1976, pp. 589-593.

[30] Platou, A.S., "The Magnus Force on Rotating Cylinder in Transonic Crossflows," BRL Rept. 1150, Sept. 1961.

[31] Murthy, V.S. and Rose, W.C., "Detailed Measurements on a Circular Cylinder in Crossflow," *AIAA Journal,* Vol. 16, June 1978, pp. 549-550.

[32] Ericsson, L.E., "Unsteady Aerodynamics of Separating and Reattaching Flow on Bodies of Revolution," *Recent Research on Unsteady Boundary Layers,* Vol. 1, IUTAM Symposium, Laval University, Quebec, May 24-28, 1971, pp. 481-512.

[33] Robertson, J.E. and Chevalier, H.L., "Characteristics of Steady-State Pressures on the Cylindrical Portion of Cone-Cylinder Bodies at Transonic Speeds," AEDC TDR 63-104, Aug. 1963.

[34] Ericsson, L.E., "Loads Induced by Terminal-Shock Boundary-Layer Interaction on Cone-Cylinder Bodies," *Journal of Spacecraft and Rockets,* Vol. 7, Sept. 1970, pp. 1106-1112.

[35] Hall, I.M., Rogers, E.W.E., and Davies, B.M., "Experiments with Inclined Blunt-Nosed Bodies at M=2.45," ARC R&M 3128, ARC Great Britain, Aug. 1957.

[36] Thomson, K.D., "The Estimation of Viscous Normal Force, Pitching Moment, Side Force, and Yawing Moment on Bodies of Revolution at Incidences up to 90°," WRE-Report-782, Australia, Oct. 1972.

[37] Mifsud, L., "Caracteristiques Aerodynamiques des Corps de Revolution Munis D'Ailes d'Allongements Divers," Paper 19, AGARD CP-247, Sept. 1978.

[38] Kruse, R.L., "Influence of Spin Rate on Side Force of an Axisymmetric Body," *AIAA Journal,* Vol. 16, April 1978, pp. 415-416.

[39] Jacobson, I.D., "Boundary-Layer Distortion on a Spinning Cone," *AIAA Journal,* Vol. 11, March 1973, pp. 395-396.

[40] Ericsson, L.E., "Transition Effects on Slender Vehicle Stability and Trim Characteristics," *Journal of Spacecraft and Rockets,* Vol. 11, Jan. 1974, pp. 3-11.

[41] Ericsson, L.E., "Nonlinear Hypersonic Viscous Crossflow Effects on Slender Vehicle Dynamics," *AIAA Journal,* Vol. 17, June 1979, pp. 586-593.

[42] Tobak, M., Schiff, L.B., and Peterson, V.L., "Aerodynamics of Bodies of Revolution in Coning Motion," *AIAA Journal,* Vol. 7, Jan. 1969, pp. 95-99.

[43] Schiff, L.B. and Tobak, M., "Results from a New Wind-Tunnel Apparatus for Studying Coning and Spinning Motions of Bodies of Revolution," *AIAA Journal,* Vol. 8, Nov. 1970, pp. 1953-1958.

[44] Mack, L.M., "Linear Stability Theory and the Problem of Supersonic Boundary-Layer Transition," *AIAA Journal,* Vol. 13, March 1975, pp. 278-289.

[45] Briggs, M.M., Clark, W.H., and Peoples, J.R., "Occurrence and Inhibition of Large Yawing Moments During High Incidence Flight of Slender Missile Configurations," *Journal of Spacecraft and Rockets,* Vol. 10, Aug. 1973, pp. 510-519.

[46] Orlik-Rückemann, K.J., "Dynamic Stability Testing in Wind Tunnels," Paper 1, AGARD CP-235, AGARD Meeting on Dynamic Stability Parameters, Athens, Greece, Sept. 25-28, 1978.

[47] Uselton, J.C., "Aerodynamic Characteristics of High Fineness Ratio Model with Various Spin Rates at M=3.0 and 5.0," AEDC TR 66-177, Sept. 1966.

[48] Ericsson, L.E., "A Summary of AGARD FDP Meeting on Dynamic Stability Parameters," Paper 2, AGARD CP-260 AGARD Symposium on Stability and Control, Ottawa, Canada, Sept. 25-28, 1978.

[49] Keener, E.R. and Taleghani, J., "Wind Tunnel Investigations of the Aerodynamic Characteristics of Five Forebody Models at High Angles of Attack at Mach Numbers from 0.25 to 2," NASA TM X-73,076, Dec. 1975.

[50] Keener, E.R., Chapman, G.T., Cohen, L., and Taleghani, J., "Side Forces on Forebodies at High Angles of Attack and Mach Numbers from 0.1 to 0.7. Two Tangent Ogives, Paraboloid and Cone," NASA TM X-3438, Feb. 1977.

[51] Keener, E.R., "Flow Separation Patterns on Symmetric Forebodies at High Incidence," AIAA Paper 80-1557, Danvers, Mass., Aug. 1980.

[52] Bird, J.D., "Tuft-Grid Surveys at Low Speeds for Delta Wings," NASA TN D-5045, Feb. 1969.

[53] Rainbird, W.J., Crabbe, R.S., Peake, D.J., and Meyer, R.F., "Some Examples of Separation in Three-Dimensional Flows," *Canadian Aeronautics and Space Journal,* Vol. 12, Dec. 1966, pp. 409-423.

[54] Keener, E.R. and Chapman, G.T., "Similarity in Vortex Asymmetries Over Slender Bodies and Wings," *AIAA Journal,* Vol. 15, Sept. 1977, pp. 1370-1372.

[55] Shanks, R.E., "Low Subsonic Measurements of Static and Dynamic Stability Derivatives of Six Flat-Plate Wings Having Leading Edge Sweep Angles of 70° to 84°," NASA TN D-1827, July 1963.

[56] Wendtz, W.H. and Kohleman, D.L., "Vortex Breakdown on Slender Sharp-Edged Delta Wings," AIAA Paper 69-778, July 1969.

[57] Ericsson, L.E. and Reding, J.P., "Approximate Nonlinear Slender Wing Aerodynamics," *Journal of Aircraft,* Vol. 14, Dec. 1977, pp. 1197-1204.

[58] Maltby, R.L. and Peckham, D.H., "Low Speed Flow Studies of the Vortex Patterns Above Inclined Slender Bodies Using a New Smoke Technique," RAE-AEO-TN-2482, ARC Great Britain, March 1957.

[59] Reding, J.P. and Ericsson, L.E., "Review of Delta Wing Space Shuttle Vehicle Dynamics," NASA CR-115357, Oct. 1971.

[60] Polhamus, E.C., "Predictions of Vortex-Lift Characteristics by a Leading-Edge Suction Analogy," *Journal of Aircraft,* Vol. 8, April 1971, pp. 193-199.

[61] Lowson, M.V., "Some Experiments with Vortex Breakdown," *Journal of the Royal Aeronautical Society,* Vol. 68, May 1964, pp. 343-346.

[62] Sarpkaya, T., "Separated Flow About Lifting Bodies and Impulsive Flow About Cylinders," *AIAA Journal,* Vol. 4, March 1966, pp. 414-420.

[63] Atraghji, E., "A Method for Estmating the Loading Distribution on Long Slender Bodies of Revolution at High Incidence in Incompressible Flow," Paper 14, AGARD CP-204, AGARD Symposium on Prediction of Aerodynamic Loading, Ames Research Center, Moffett Field, Calif., Sept. 1976.

[64] Deffenbaugh, F.D. and Marshall, F.J., "Time Development of the Flow about an Impulsively Started Cylinder," *AIAA Journal,* Vol. 14, July 1976, pp. 908-913.

[65] Fiechter, M., "Kegelpendelung, Autorotation und Wirbelsysteme schlanker Flugkörper," *Z. Flugwiss,* Vol. 20, Aug. 1972, pp. 281-292.

[66] Lamont, P.J. and Hunt, B.L., "Out-of-Plane Force on a Circular Cylinder at Large Angles of Inclination to a Uniform Stream," *Aeronautical Journal,* Vol. 69, Jan. 1973, pp. 41-45.

[67] Wardlaw, A.B. Jr., "Prediction of Normal Force, Pitching Moment, and Yawing Force on Bodies of Revolution at Angles of Attack up to 50 Degrees Using a Concentrated Vortex Flow-Field Model," NOL TR 73-209, Oct. 1973.

[68] Jorgensen, L.H., "Prediction of Static Aerodynamic Characteristics for Space Shuttle Like and Other Bodies at Angles of Attack from 0° to 180°," NASA TN D-6996, Jan. 1973.

[69] Kubin, J.S., "An Analysis of Steady Asymmetric Vortex Shedding from a Missile at High Angles of Attack," AD-774390, Air Force Institute of Technology, Nov. 1973.

[70] Wardlaw, A.B. Jr., "Prediction of Yawing Force at High Angle of Attack," *AIAA Journal,* Vol. 12, Aug. 1974, pp. 1142-1144.

[71] Fidler, J.E. and Bateman, M.C., "Asymmetric Vortex Effects on Missile Configurations," *Journal of Spacecraft and Rockets,* Vol. 12, Nov. 1975, pp. 674-681.

[72] Wardlaw, A.B. Jr. and Morrison, A.M., "Induced Side Forces at High Angles of Attack," NSWC/WOL/TR 75-176, Nov. 1975.

[73] Lamont, P.J. and Hunt, B.L., "Prediction of Aerodynamic Out-of-Plane Forces on Ogive-Nosed Circular Cylinders," *Journal of Spacecraft and Rockets,* Vol. 14, Jan. 1977, pp. 38-44.

[74] Reding, J.P. and Ericsson, L.E., "Maximum Side Forces and Associated Yawing Moments on Slender Bodies," *Journal of Spacecraft and Rockets,* Vol. 17, Nov.-Dec. 1980, pp. 515-521.

[75] Ericsson, L.E. and Reding, J.P., "Vortex-Induced Asymmetric Loads in 2-D and 3-D Flows," AIAA Paper 80-0181, Pasadena, Calif., Jan. 1980.

[76] Kamiya, N., Suzuky, S., and Nishi, T., "On the Aerodynamic Force Acting on a Circular Cylinder in the Critical Range of the Reynolds Number," AIAA Paper 79-1475, July 1979.

[77] Jones, G.W. Jr., Cincotta, J.C., and Walker, R.W., "Aeodynamic Forces on a Stationary and Oscillating Circular Cylinder at High Reynolds Numbers," NASA TR R-300, Feb. 1969.

[78] Ericsson, L.E. and Reding, J.P., "Dynamic Stall of Helicopter Blades," *Journal of the American Helicopter Society,* Vol. 17, Jan. 1972, pp. 10-19, *Journal of Aircraft,* Vol. 12, Feb. 1975, pp. 86-92.

[79] Ericsson, L.E., "Dynamic Effects of Shock-Induced Flow Separation." [80] Ericsson, L.E. and Reding J.P., "Scaling Problems in Dynamic Tests of Aircraft-Like Configurations," Paper 25, AGARD CP-227, AGARD Conference on Unsteady Aerodynamics, Ottawa, Can., Sept. 26-28, 1977.

[81] Ericsson, L.E. and Reding, J.P., "Renolds Number Criticality in Dynamic Tests," AIAA Paper 78-166, Jan. 1978.

[82] Bearman, P.W., "On Vortex Shedding from a Circular Cylinder in the Critical Reynolds Number Regime," *Journal of Fluid Mechanics,* Vol. 37, Pt. 3, 1969, pp. 577-585.

[83] Ericsson, L.E. and Reding, J.P., "Analytic Prediction of Dynamic Stall Characteristics," AIAA Paper 72-682, June 1972.

[84] Carr, L.W., McAllister, K.W., and McCroskey, W.J., "Analysis of the Development of Dynamic Stall Based on Oscillating Experiments," NASA TN D-8382, Jan. 1977.

[85] AGARD FDP Meeting on Dynamic Stability Parameters, AGARD CP-235, Athens, Greece, May 22-24, 1978.

[86] Krause, R.L., Keener, E.R., Chapman, G.T., and Claser, G., "Investigation of the Asymmetric Aerodynamic Characteristics of Cylindrical Bodies of Revolution with Variations in Nose Geometry and Rotational Orientation at Angles of Attack to 58° and Mach Numbers to 2," NASA TM 78533, Sept. 1979.

[87] Lamont, P.J., "Pressure Distributions on an Ogive-Cylinder at High Angles of Attack with Laminar, Transitional, or Turbulent Separation," AIAA Paper 80-1556, Aug. 1980.

[88] Fidler, J.E., "Active Control of Asymmetric Vortex Effects," AIAA Paper 80-0182, Jan. 1980.

[89] Swanson, W.M., "The Magnus Effect: A Summary of Investigations to Date," *Journal of Basic Engineering,* Sept. 1961, pp. 461-470.

[90] Wallis, R.A., "Boundary Layer Transition at the Leading Edge of Thin Wings and its Effect on General Nose Separation," *Advances in Aeronautical Sciences,* Proceedings of the Second International Congress in the Aeronautical Sciences, Zurich, Sept. 12-16, 1970, pp. 161-184.

[91] Wallis, R.A., "The Turbulent Boundary Layer on the Articulated Nose of a Thin Wing Provided with Air Jets," ARL Aero Note 141, Aeronautical Research Laboratories, Australia, Oct. 1954.

[92] Keener, E.R., private communication of unpublished Flow Visualization Results, Oct. 1979.

[93] Sharir, D., Portnoy, H., and Rom, J., "A Study of the Effects of Jets Injected from a Slender Body of Revolution on the Side Forces Acting on it at Large Angles of Attack in Low Speeds," Technion Israel Institute of Technology, Dept. of Aero. Eng., TAE 337, May 1978.

[94] Ericsson, L.E. and Reding, J.P., "Unsteady Airfoil Stall, Review and Extension," *Journal of Aircraft,* Vol. 8, Aug. 1971, pp. 609-616.

[95] Ericsson, L.E. and Reding, J.P., "Dynamic Stall Analysis in Light of Recent Numerical and Experimental Results," *Journal of Aircraft,* Vol. 13, April 1976, pp. 248-255.

[96] Ericsson, L.E. and Reding, J.P., "Quasi-Steady and Transient Dynamic Stall Characteristics," Paper 24, AGARD CP-204, AGARD Symposium on Prediction of Aerodynamic Loading, Moffet Field, Calif., Sept. 27-29, 1976.

[97] Ericsson, L.E. and Reding, J.P., "Dynamic Stall at High Frequency and Large Amplitude," *Journal of Aircraft,* Vol. 17, March 1980, pp. 136-142.

[98] Peake, D.J. and Owen, F.K., "Control of Forebody Three-Dimensional Flow Separations," Paper 15, AGARD CP-262, May 1979.

[99] Peake, D.J., Owen, F.K., and Johnson, D.A., "Control of Forebody Vortex Orientation to Alleviate Side Forces," AIAA Paper 80-0183, Jan. 1980.

[100] Skow, A.M., Moore, W.A., and Lorincz, D.J., "Forebody Vortex Blowing—A Novel Control Concept to Enhance Departure/Spin Recovery Characteristics of Fighter and Trainer Aircraft," Paper 24, AGARD CP-262, May 1979.

[101] Tobak, M., "On Local Inflexional Instability in Boundary-Layer Flows," ZAMP, Vol. 24, 1973, pp. 330-354.